



Published in final edited form as:

*Clin Cancer Res.* 2009 April 1; 15(7): 2352–2360. doi:10.1158/1078-0432.CCR-08-2082.

## Mathematical Modeling of Herpes Simplex Virus Distribution in Solid Tumors: Implications for Cancer Gene Therapy

Wilson Mok<sup>1,2</sup>, Triantafyllos Stylianopoulos<sup>1</sup>, Yves Boucher<sup>1</sup>, and Rakesh K. Jain<sup>1</sup>

<sup>1</sup> Department of Radiation Oncology, Edwin L. Steele Laboratory, Massachusetts General Hospital, Harvard Medical School, Boston, Massachusetts

<sup>2</sup> Department of Chemical Engineering, Massachusetts Institute of Technology, Cambridge, Massachusetts

### Abstract

**Purpose**—Although oncolytic viral vectors show promise for the treatment of various cancers, ineffective initial distribution and propagation throughout the tumor mass often limit the therapeutic response. A mathematical model is developed to describe the spread of herpes simplex virus from the initial injection site.

**Experimental Design**—The tumor is modeled as a sphere of radius  $R$ . The model incorporates reversible binding, interstitial diffusion, viral degradation, and internalization and physiologic parameters. Three species are considered as follows: free interstitial virus, virus bound to cell surfaces, and internalized virus.

**Results**—This analysis reveals that both rapid binding and internalization as well as hindered diffusion contain the virus to the initial injection volume, with negligible spread to the surrounding tissue. Unfortunately, increasing the dose to saturate receptors and promote diffusion throughout the tumor is not a viable option: the concentration necessary would likely compromise safety. However, targeted modifications to the virus that decrease the binding affinity have the potential to increase the number of infected cells by 1.5-fold or more. An increase in the effective diffusion coefficient can result in similar gains.

**Conclusions**—This analysis suggests criteria by which the potential response of a tumor to oncolytic herpes simplex virus therapy can be assessed. Furthermore, it reveals the potential of modifications to the vector delivery method, physicochemical properties of the virus, and tumor extracellular matrix composition to enhance efficacy.

Viral vectors offer a promising approach to cancer treatment. Methods of antitumor efficacy can include cell lysis, cytotoxicity of viral proteins, induction of an immune response, and expression of a cytotoxic transgene. Oncolytic viral therapy—treatment with viruses that have been genetically modified to selectively replicate in cancer cells but not nonneoplastic cells—is a rapidly developing cancer gene therapy platform that can exhibit each of these antitumor properties. Two of the most actively investigated viruses, adenovirus and herpes simplex virus (HSV), have shown systemic safety and efficacy in various clinical applications (1).

Requests for reprints: Rakesh K. Jain, E.L. Steele Laboratory, Massachusetts General Hospital, 100 Blossom Street, Cox 7, Boston, MA 02114. Phone: 617-726-4083; Fax: 617-724-1819; jain@steele.mgh.harvard.edu.

#### Disclosure of Potential Conflicts of Interest

No potential conflicts of interest were disclosed.

**Note:** Supplementary data for this article are available at Clinical Cancer Research Online (<http://clincancerres.aacrjournals.org/>).

Although viral gene therapy vectors show remarkable biological specificity and activity for the treatment of solid tumors, they suffer compared with conventional chemotherapeutics in one main respect: intratumor distribution. Viruses are orders of magnitude larger than small molecule chemotherapeutics (<1 nm versus 50–200 nm) and encounter severe transport limitations in the tumor interstitium (2). The limited penetration of large vectors from the injection site or the vasculature has been well-documented (3–5). The tumor extracellular matrix most likely plays an important role in the distribution of viral vectors within tumors (6,7). To properly assess the therapeutic potential of a viral cancer gene therapy vector, as well as devise optimal delivery methods, a detailed understanding of the root causes of limited vector distribution is needed.

Mathematical modeling offers a useful method to explore this issue and guide experimental strategies to improve viral vector distribution and thus efficacy. Several models of oncolytic viral therapy exist in the literature (8–10). Although extremely informative, these models focus on the role of various biological processes such as the immune response and the cytotoxicity, infectivity, and burst size of the virus. In addition, they compare how different treatment/delivery schemes—manifested as initial intratumor viral distribution—affect the ability to control tumor growth with oncolytic viral therapy. The present investigation aims to address the more fundamental questions of how these initial distributions arise and what physicochemical characteristics of the virus are responsible. We consider the role of viral binding, internalization, diffusion, and degradation and explore the potential improvements in distribution with various modifications to both the virus and tumor. Furthermore, although the previous models describe the behavior of adenoviral vectors, this study focuses on HSV (MGH2), which also shows great potential in tumor treatment.

Experiments are done in this study to determine the rate constants for viral degradation (via hydrolysis) and cell surface binding and the concentration of heparan sulfate on the surface of tumor cells. Values for the volume and concentration of virus after intratumor infusion and the effective diffusion coefficient of viral particles in the tumor are estimated from our previous work (6,11). Other parameters have been estimated from the literature. The model shows that intratumorally infused virus will spread minimally from the site of injection, a consequence of rapid cell surface binding and limited diffusion. However, various modifications to the tumor and virus can markedly improve the distribution of virus in the tumor.

## Materials and Methods

### Mathematical model

The tumor is modeled as a sphere of radius  $R$ . Diffusion-reaction equations describe the interstitial concentration of virus as a function of time and radial position. Diffusion in the interstitial compartment, binding and uptake of HSV particles to cells, and degradation of both free and bound viral particles via hydrolysis are the processes described (Fig. 1). Three species considered are as follows: free interstitial virus, virus bound to cell surfaces, and internalized virus.

HSV binding to the cell surface and subsequent internalization is not mediated by a simple single ligand-single receptor interaction. Rather, it is a multistep process that involves several viral envelope glycoproteins (12) and assumptions were made to facilitate mathematical modeling. Cell surface binding has been found to be primarily mediated by the interaction of glycoproteins gB and gC with heparan sulfate (13–15). A comparison of binding affinities (16,17) and separate mutant virion analyses (18,19) suggest that gC binding to heparan sulfate is the primary mechanism for cell surface attachment of HSV. Thus, we have modeled the binding of HSV to cells as an interaction between the glycoprotein gC and cell surface heparan sulfate. A second ligand-receptor interaction (gD-HVEM) facilitates internalization.

For the model formulation, we also assume that there is no limit to the number of virus that can be internalized by a single cell in accordance with models for antibody distribution in tumors (20). A limit for the number of internalized virus must, however, exist. This limit varies considerably among different cell types but every cell, which is permissive for viral replication, is expected to uptake several hundreds of virus before being saturated.<sup>3</sup> Given the number of virus that can be internalized and the fact that the multiplicity of infection is relatively low (usually <100 virus particles), saturation of the cells does not seem likely to happen.

The concentration profile for free (interstitial), and bound virus are given by

$$\frac{\partial C_I}{\partial t} = \frac{D}{r^2} \frac{\partial}{\partial r} \left( r^2 \frac{\partial C_I}{\partial r} \right) - \frac{k_{on} C_I (C_{HS} - a C_B)}{\phi} + k_{off} C_B - k_d C_I \quad (1)$$

$$\frac{\partial C_B}{\partial t} = \frac{k_{on} C_I (C_{HS} - a C_B)}{\phi} - k_{off} C_B - k_d C_B - k_{int} C_B \quad (2)$$

where  $C_I$  and  $C_B$  are the concentrations of free and bound virus, respectively (M);  $t$  is the time (s);  $r$  is the radial distance (cm);  $D$  is the effective diffusion coefficient of virus in the interstitial space ( $\text{cm}^2\text{s}^{-1}$ );  $k_{on}$  is the second-order rate constant for binding of free virus ( $\text{M}^{-1}\text{s}^{-1}$ );  $k_{off}$  is the first-order rate constant for dissociation of bound virus from the cell surface ( $\text{s}^{-1}$ );  $\phi$  is the volume fraction available to virus in the tumor;  $C_{HS}$  is the concentration of cell surface receptors (M);  $a$  is the number of receptors sterically blocked by the binding of each viral particle;  $k_d$  is the rate constant for degradation of the virus ( $\text{s}^{-1}$ ), assumed to be the same for both bound and free virus; and  $k_{int}$  is the rate constant of internalization of the bound virus. The rate of change of the internalized virus is assumed to follow a first-order kinetics, i.e.,  $\partial C_{int}/\partial t = k_{int} C_B$ . Therefore, the concentration of the internalized virus can be calculated by the solution of the system of the two equations.

The boundary conditions are specified by spherical symmetry at the center of the tumor and a virus sink at the edge of the tumor:

$$\begin{aligned} \frac{\partial C_I}{\partial r} &= 0 \text{ at } r=0 \\ C_I &= 0 \text{ at } r=R. \end{aligned}$$

The initial conditions are

$$\begin{aligned} C_I &= C_0 \text{ for } r \leq \rho \\ C_I &= 0 \text{ for } r > \rho \end{aligned}$$

with no bound virus throughout the tumor. These conditions reflect a uniform initial concentration of virus in the center of the tumor after direct intratumor injection, a common approach in the treatment of solid tumors (21). The injection volume is spherical with a radius of  $\rho$ . The differential equations were nondimensionalized (see Supplementary Model Description) and solved simultaneously using a numerical finite difference method in Matlab.

<sup>3</sup>P. Grandi, personal communication.

### Choice of tumor and initial viral distribution

The baseline parameter values for the model are given in Table 1. As we are interested in determining the transport limitations specifically in high collagen tumors, we used as our model tumor HSTS26T, a human soft tissue sarcoma that we have previously shown has elevated levels of collagen (7). The tumor radius was set to 0.05 cm based on our previous studies (22,23). The radius of initial viral distribution into a fibrous tumor was measured in our previous work (6) and was taken to be 0.025 cm. In that study, the area of initial viral distribution was quantified by multiphoton imaging of fluorescently labeled HSV vectors at the injection site.

### Estimation of transport parameters

The effective diffusion coefficients of particles the size of HSV have not been measured in tumors with high collagen content. However, we previously measured the diffusion coefficient of particles up to ~40 nm diameter in fibrous melanoma and sarcoma xenografts (24) and of ~150 nm diameter liposomes in tumors with relatively little collagen (11,25). By extrapolation the effective diffusion coefficient of HSV particles in tumors with high collagen content should be  $5 \times 10^{-10} \text{ cm}^2\text{s}^{-1}$ . For validation, we also estimated the diffusion coefficient based on the effective medium model for hindered diffusion of a solid sphere (26,27). In separate studies, we have previously found the Darcy permeability ( $K$ ) of HSTS26T tumors to be  $3 \text{ nm}^2$  (7) and  $50 \text{ nm}^2$  (28). We should note that the Darcy permeability of collagen gels with similar collagen content to HSTS26T tumors (30 mg/mL interstitial matrix) was found to be  $40 \text{ nm}^2$  after correction for the effect of cells (29). Assuming the diffusion coefficient of HSV particles in solution is equivalent to that of similarly sized liposomes, this leads to calculated diffusion coefficients of  $2 \times 10^{-9} \text{ cm}^2\text{s}^{-1}$  ( $K = 50 \text{ nm}^2$ ) and  $2 \times 10^{-10} \text{ cm}^2\text{s}^{-1}$  ( $K = 3 \text{ nm}^2$ ). Thus, our extrapolated value from the *in vivo* data seems reasonable.

### Estimation of kinetic parameters

We estimated the rate constant for degradation of HSV particles in the tumor interstitium by measuring the rate of degradation in HSTS26T conditioned media and fitting to a first-order kinetic model (Supplementary Fig. S1). Briefly, replication competent HSV (MGH2) particles were incubated with 24-h conditioned media from HSTS26T cells at several concentrations at 37°C. At various time points, the medium was frozen in a dry ice/ethanol bath. The concentration of viable viral particles at each time point was determined by titrating each sample with HSTS26T cells. The rate constant for degradation was estimated by fitting the data to a first-order rate equation. Incubation was done in duplicate and titration of both samples in triplicate, and the average values were used in the analysis. It seems that proteins secreted by tumor cells can degrade HSV because the half-time for degradation is ~4.25 h when incubated with conditioned media, compared with ~24 h when incubated with PBS. Lacking information for the degradation rate of bound virus, we assumed that it happens at the same rate as the degradation rate of the virus in the solution.

The cell surface heparan sulfate concentration was determined experimentally for HSTS26T cells using a dimethyl methylene blue dye assay following the manufacturer's protocol (Biocolor), and it is given in Table 1. The cell density was estimated to be  $7.23 \times 10^8$  cells/mL ( $1.2 \times 10^{-12} \text{ M}$ ) based on Thurber et al. (20). To determine the number of heparan sulfate molecules blocked by the binding of a single viral particle to the cell surface, we first needed to determine the number of viral particles that can bind to a single cell. We modeled viral particles and cells as spheres of 150 nm and 10  $\mu\text{m}$  diameter, respectively, and assumed simple cubic packing of virus on the cell surface. This analysis showed that virus, rather than receptor, is limiting for HSV binding to cells ( $2.25 \times 10^4$  viruses per cell versus  $1.0 \times 10^7$  heparan sulfate molecules per cell). Although simple cubic packing most likely cannot be achieved due to steric effects and the presence of other proteins on the cell surface, virus internalization occurs very rapidly ( $t_{1/2}$ , ~8 min; ref. 30) and frees space on the cell surface for other HSV particles to

bind. As a conservative estimate, the calculated value for the number of viral particles that can bind a single cell was reduced by a factor of 2. The number of heparan sulfate molecules blocked by a single binding event was then estimated based on the total amount of heparan sulfate per cell. Steric effects are also expected to slow down the internalization process, and thus, for the calculation of the rate constant of internalization, the half time was taken to be 20 min, 2.5 times larger than *in vitro* measurements.

The rate constant for dissociation of bound virus from cell surface heparan sulfate was estimated from a kinetic analysis of the binding of soluble gC to immobilized heparan sulfate using surface plasmon resonance (16). The kinetic data fit well with a 1:1 model (one molecule of gC binding to one molecule of heparan sulfate). The dissociation rate constant for this process was measured at 25°C. To adjust to the physiologic temperature of 37°C, we estimated the effect of temperature on the binding rate constant using published kinetic analyses of a variety of other proteins (31–34). From these data, we assumed an increase of  $\sim 1.0$  in  $\ln(k_{\text{off}}/T)$  for the temperature change of interest. Although Rux et al. (16) measured the kinetic rate constant for individual gC molecules, we applied them to HSV particles. Based on the spherical nature of the HSV particle, we assumed that its attachment to the cell surface occurs at the pole, due to the interaction of a single gC molecule with heparin sulfate.

Although Rux et al. (16) also measured the association rate constant for binding of soluble gC to heparan sulfate, it was difficult to convert this value to a rate constant for HSV particles. It is not clear whether the affinity of viral particles scales with the number of gC molecules on its surface. To more accurately estimate the association rate constant, we experimentally assessed the binding of HSV particles to HSTS26T cells in solution (Supplementary Fig. S2). Briefly, replication competent HSV particles were incubated with HSTS26T cells in suspension with gentle agitation. At various time points, cells were pelleted by centrifugation and the supernatant immediately collected and frozen in a dry ice/ethanol bath. The concentration of viral particles at each time point was determined by titrating with HSTS26T cells. The association rate constant was estimated by fitting the data to a second-order rate equation.

The values of the rate constants were determined based on the MGH2 type of HSV. Other common types of HSV, such as G207 and G47 $\Delta$ , are of the same size as MGH2 and have identical envelopes. Therefore, we expect that the rates of diffusion, binding, internalization, and degradation of these viruses to be similar to the corresponding rates of MGH2, and thus, our model predictions should be applicable for these types of HSV. Another common type of HSV, the NV1020, has a similar size and envelope with the MGH2 but also has a 5.2-kbp insertion of an HSV-2 surface glycoprotein, which differentiate it from MGH2, and thus, its efficiency of infection is probably different.

### Estimation of volume fraction and viral concentration

There are no published measurements of the volume fraction of HSV particles or other similarly sized particles in tumors. However, Krol et al. (35) developed an *ex vivo* method to measure the volume fraction in tumors and determined the value for dextrans of various sizes. We estimated the volume fraction by using the value they measured for the largest dextran ( $2 \times 10^6$  MW) in s.c. MCA-R fibrosarcomas.

The initial intratumor viral concentration is taken from our experiments done with direct injections of the oncolytic HSV vector MGH2 to treat a fibrous melanoma (6). The concentration of virus in the tumor can be estimated because both the viral dose,  $1 \times 10^6$  plaque-forming unit, and the volume of virus distribution—as determined by imaging of the fluorescently labeled viral particles directly after injection—are known. It is important to note that plaque-forming unit is not a direct measure of total number of viral particles. In the assay

for determining plaque-forming unit, plaque formation depends on multiple steps beyond simply binding and internalization of the viral particle. Thus, not every viable HSV particle (as defined in this model) will lead to plaque formation. The total number of HSV particles can range from 3 to 100 times the plaque-forming unit, as determined by PCR, PicoGreen staining analysis of the wild-type HSV.<sup>4</sup> Clearly, this will be dependent on the experiment, cell line, and virus preparation. As an approximation, we have estimated the total viral concentration from the plaque-forming unit by using a factor of 50.

## Results

### Baseline simulations

We present our model results in terms of the Damkohler number, which represents the ratio of the time scale for diffusion relative to various kinetic processes. Using the baseline values, the Damkohler numbers for association ( $Da_{on}$ ), dissociation ( $Da_{off}$ ), degradation ( $Da_d$ ), and internalization ( $Da_{int}$ ) were calculated (see Supplementary Model Description). All four Damkohler numbers are much greater than 1 ( $Da_{on} = 8.7 \times 10^6$ ,  $Da_{off} = 4.0 \times 10^4$ ,  $Da_d = 2.4 \times 10^2$ ,  $Da_{int} = 2.9 \times 10^3$ ), signifying that the processes of binding, degradation, and internalization occur much more rapidly than diffusion (Fig. 2A–C). Most of the virus binds to cell surfaces and is internalized very rapidly. Four hours after viral injection >90% of the initial amount of virus was internalized and the rest degraded because there is no free or bound virus left (Fig. 2A–C). Additionally, there is little virus diffusion in the adjacent tumor tissue; at 4 hours, <3% of the remaining virus is beyond the initial injection volume. To confirm that the distinctive profile is a consequence of rapid binding and internalization, the model simulation was also done without both binding and internalization. The virus diffuses further in the tumor, and after 4 hours, which is the half time of viral degradation, half of the virus is degraded (Supplementary Fig. S3).

### Sensitivity analysis

Next, we did a sensitivity analysis to determine the relative importance of each parameter and to gauge the ability of various virus and tumor modifications to improve intratumor distribution and therapeutic efficacy (Table 2). To compare different simulations, various indices were considered. The total number of internalized viral particles in both the initial distribution volume (“virus inside”) and the adjacent, initially uninfected region (“virus outside”) were calculated. The values normalized to the baseline simulation for each of the two species are also given, serving as a better measure of the relative change induced by each modification. We assessed the amount of viral spread from the initial injection site by calculating the volume of adjacent space that contains internalized virus (“volume spread”). We chose as our threshold internalized virus concentration 1% of the initial injection concentration ( $1.27 \times 10^{-11}$  M). This concentration corresponds to ~10 viral particles per cell. The entry of 1 viral particle in the cell nucleus can cause cell death (36); thus, the uptake of 10 particles will likely lead to cell infection. The volume spread was calculated at each time point and the maximum value was chosen to best reflect the volume of the tumor that is infected with virus. A description of each of the simulations follows.

### Binding kinetics

We first examined the effect of changes in virus binding characteristics on spatial distribution. We analyzed the extent to which a decrease in affinity to heparan sulfate would improve distribution. A 10-fold decrease in the affinity increases negligibly the amount of internalized virus in the adjacent space and the spread volume (Fig. 3A). This change in the affinity constant

---

<sup>4</sup>P. Grandi, personal communication.

was chosen to reflect possible changes to the virus itself. Rux et al. (16) found that deletion of residues 33 to 123 of gC results in an order of magnitude increase in its  $K_D$ . Furthermore, it has been shown that gB-heparan sulfate is the second strongest interaction between HSV and cells, with a binding affinity that is an order of magnitude lower than for gC (16,17). Thus, a 10-fold decrease in the affinity constant approximates the change that would occur if gC is modified or deleted.

Beyond gC and gB, the interaction of other viral envelope glycoproteins with cell surfaces is less well-studied. It has been found that the binding affinity of gD with its cell surface receptor is an order of magnitude lower than for gB-heparan sulfate, and two orders of magnitude lower than for gC-heparan sulfate (37). Thus, we examined the effect of a two orders of magnitude decrease in the affinity, which would reflect changes to both gC and gB. This leads to a >50% increase in the spread volume (Fig. 3A). As expected, the amount of internalized virus in the initial injection area decreases as a greater fraction is free and diffuses out of this volume. However, there is still enough virus per cell in this region to cause cell infection.

When changes to the dissociation constant (i.e.,  $Da_{off}$ ) were analyzed, we found proportional and opposite effects when compared with changes in the association constant (i.e.,  $Da_{on}$ ). Thus, these results are not displayed in Table 2. We should also note that a change in  $Da_{on}$  can reflect a change in either  $k_{on}$  or  $C_{HS}$ . Thus, binding affinity can be reduced by changing the virus, as mentioned above, or by modulating the levels of heparan sulfate receptors.

### Degradation

Our experiments showed that the  $t_{1/2}$  for degradation of HSV particles at 37°C in tumor cell conditioned media is ~4 hours, whereas  $t_{1/2}$  is ~ 24 hours in PBS. However, these *in vitro* experiments may not completely capture the conditions *in vivo*, where the concentration of extracellular factors may be different. It is therefore important to analyze the sensitivity of the model to this parameter. Virus binding and internalization takes place much faster than degradation and is the main cause of loss of bound virus from the system. When the degradation rate constant is increased by a factor of 10, the amount of internalized virus decreases by ~40% because now, the degradation and internalization rate constants are of the same order of magnitude, whereas the spread volume is decreased by only 6% (Fig. 3B).

Conversely, decreasing the virus half-life by a factor of 10 did not change the concentration profile and the spread volume significantly compared with the baseline simulation (Fig. 3B). This is because the virus is internalized rapidly and it has no time for degradation.

### Internalization

Based on *in vitro* studies (30), we estimated the half time of virus internalization to be 20 minutes, an order of magnitude faster than the rate of degradation. As a result, when the virus is bound to the cell surface, it is internalized rapidly and frees up space for more viruses. This is the reason that for the baseline simulation almost all the virus is internalized inside the injection volume and only a small proportion is able to diffuse in the adjacent tumor volume. We expect, however, that as more and more virus is internalized, the ability of the cell to take up more viruses is decreasing. A 10- and 100-fold decrease of the internalization rate reduces the amount of internalized virus by 40% and 90%, respectively. However, the volume spread of the virus increases only by 5% (Fig. 3B). Therefore, changing the internalization rate of viral particles does not alter virus distribution significantly.

### Diffusion

Altering the effective diffusion coefficient can have an effect on the distribution of virus in the tumor. Our previous work has shown that the effective diffusion coefficient in tumors correlates

negatively with collagen content (7). In this model, we have chosen our effective diffusion coefficient to reflect transport in a collagen-rich fibrosarcoma. Thus, we have chosen a particularly low diffusion coefficient. Based on a comparison of the effective diffusion coefficient of various tracer molecules in tumors with high and low levels of collagen (11), we believe that a 20-fold increase in  $D$  more accurately reflects the conditions in less fibrous solid tumors. Furthermore, based on previous work, we estimate that this increase in diffusion coefficient is possible for large particles such as HSV in high-collagen tumors with the addition of collagen-modulating factors (7,38). The increase in the diffusion coefficient results in a 25% increase in the amount of internalized virus outside the initial injection volume, and the spread volume increases by 18% (Fig. 3A). Thus, the model predicts that an oncolytic HSV vector would be more effective in treating a low-collagen tumor than a high-collagen one. It also suggests that matrix modification may be a useful method to improve viral vector distribution in those tumors with a significant amount of collagen and hindered diffusion.

### Volume fraction

The volume fraction of tumor accessible to virus has the potential to affect therapeutic response because it influences virus accumulation and distribution in the tumor. The variation in volume fraction for particles the size of HSV has not been determined in different tumors. However, the interstitial volume of tumors—which plays an important role in determining the available volume fraction—has been measured in various tumors and found to range from 10% to 60% (39–41). In a fibrosarcoma with an interstitial fluid space of ~50%, the accessible volume fraction for large macromolecules (molecular weight,  $>10^5$ ) was found to be  $<0.1$ . Based on these data, to approximate various tumors, we did the simulation with a 3-fold increase ( $\phi = 0.15$ ) and 3-fold decrease ( $\phi = 0.017$ ) in the volume fraction. Table 2 shows that variation of the volume fraction does not have any direct effect to the kinetics of viral distribution. However, changes in the volume fraction affect significantly the diffusion coefficient,  $D$ , of the virus, which in turn can change the distribution of the virus in the tumor.

### Initial dose

We analyzed the effect of input viral dose. A 100-fold increase in initial viral concentration resulted in nearly equivalent increases in viral concentrations inside the initial distribution, and only an 18% increase in the spread volume (Table 2). A greater than proportional increase in the amount of virus outside the initial distribution volume was observed, suggesting that we are approaching the viral concentration necessary to saturate receptors. Indeed, for a 1,000-fold increase in the viral concentration,  $<12\%$  of this virus inside the injection site is internalized (Fig. 4A) within the first 4 hours after injection. The virus behaves like a moving front of internalized virus. The final amount of virus outside the initial injection volume has been increased by  $>400$  times compared with the baseline simulation and the volume spread has increased by 60%.

### Discussion

The model has revealed some important characteristics of intratumor virus transport. The simulations show that rapid binding and internalization, and impaired diffusion limit the distribution of virus in the tumor. After injection into the interstitial space, virus will quickly bind to cells. Even in the absence of binding, diffusion is a relatively slow process due to the large size of the virus (6). The model also points to various methods of virus and tumor modification, which can enhance the efficacy of oncolytic HSV. Two such modifications are a decrease in the binding affinity via alteration of the viral envelope and an increase in the effective diffusion coefficient of virus through degradation of the tumor extracellular matrix. Model simulations with both of these modifications show significantly improved virus distribution (Table 2; Fig. 4B). Although modified HSV vectors with mutations in gC and gB

have been developed (18,19,42), these changes have yet to be incorporated into oncolytic vectors. Additionally, other envelope modifications have been developed (43). Whether these changes can improve viral spread and enhance efficacy is an exciting question that we hope will be answered in the near future.

Lowering the binding affinity improves the distribution of HSV but at the same time decreases virus binding and internalization, which is in agreement with studies for the penetration of specific antibodies in tumors (20). Our results (Table 2) show that although the binding affinity was reduced by a factor of 100, the amount of virus inside the initial injection volume was reduced by only 6%, whereas the volume spread was increased by 52%. Here, we again assumed that 1% of the initial viral concentration is sufficient to infect the cells. It is likely, however, that a low binding affinity affects the infectivity of the virus, and in this case, more viral particles may be required to kill cells.

A second approach to overcome rapid binding and enhance diffusion is to alter virus binding sites in the tissue, similar to the approach previously developed for antibodies (44). In theory, virus particles would diffuse farther but then compete for binding sites and eventually infect cells distant from the injection site. This method has the advantage of not altering the intrinsic affinity of the virus, which may have unforeseen consequences and decrease infection efficiency. As for modifications to the tumor extracellular matrix to increase diffusion, we have shown that bacterial collagenase can enhance the distribution and efficacy of oncolytic HSV in a human tumor xenograft model (6). In the future, clinically relevant approaches to degrade the matrix or block the synthesis of matrix molecules may improve the delivery of virus while avoiding unwanted secondary effects such as enhanced tumor cell invasion and metastasis.

Because the initial virus distribution in the tumor is critical for an oncolytic virus to control tumor growth, this also points to the importance of the method of viral delivery. For a direct intratumor injection, the rate and volume of infusion, tumor permeability and hydraulic conductivity, and the number of injection sites will all be key parameters. Any choice of parameter values that improves the initial distribution may enhance treatment outcome. Indeed, a study has already shown that fractionated injection of an oncolytic HSV in multiple sites is advantageous to a single injection (45). Bobo et al. (46) showed that the distribution of large molecules in the brain could be improved by prolonged infusion. They also showed that the volume of distribution increased linearly with the infusion volume. However, enhancing the distribution of therapeutics by optimizing infusion parameters may not be a viable option for many tumors. Boucher et al. (47) found that even at low flow rates, albumin infused in the center of a fibrosarcoma distributed asymmetrically from the source. Fluid accumulated in necrotic regions and at the surface of the tumor, with channels of fluid connecting these regions. The extreme stiffness of these tumors—likely due to the composition and structure of the extracellular matrix—seemed to contribute to the difficulty in obtaining uniform and widespread delivery. Given this observation, an alternative method to enhance intratumoral infusion may be to increase the permeability and hydraulic conductivity of the tumor. We have recently validated this hypothesis experimentally (24). The expression of the matrix degrading proteases matrix metalloproteinase-1 and matrix metalloproteinase-8 was shown to increase tumor hydraulic conductivity, improve the distribution of intratumorally injected oncolytic HSV vectors, and enhance overall therapeutic efficacy. Killing tumor cells (e.g., apoptosis) to create interstitial transport pathways can also increase the spread and efficacy of oncolytic HSV (48).

Our current model is limited in that it does not account for downstream events and particularly for virus replication. Modeling virus replication and the spread of viral progeny is a challenging task and was beyond the scope of the present study. The entire process of HSV replication takes ~18 to 20 hours (36). In this time interval, other events—such as tumor cell proliferation

and tumor volume change—occur, which further increase the complexity of the model. However, after cells lysis, the transport of progeny virus in the extracellular space is also hindered; hence, only adjacent cells will be infected. Characteristic of the slow diffusive transport of the virus is the fact that given the baseline value of the diffusion coefficient ( $5 \times 10^{-10} \text{ cm}^2/\text{s}$ ), it will take ~22 minutes for the virus to travel a distance equal to the size of a cell (~20  $\mu\text{m}$ ). The model results are consistent with the slow diffusion and local infection of neighboring cells, although direct spread from cell to cell through junctions likely contributes, as well (49).

The model also does not account for binding of the virus to extracellular matrix molecules or other cell surface molecules and receptors, and lacks a complete description of virus clearance, particularly via the systemic circulation, which has been found to be quite significant for intratumorally injected virus (50). The model also assumes a uniform distribution of virus in the center of the tumor after intratumor injection, ignoring the effects that matrix structures and infusion conditions can have on convective delivery during this process. Furthermore, the remarkable variations in the composition of the interstitial matrix and in the organization of the vascular network between tumor types add further complexity in the development of a complete model. For that reason, the tumor of interest has to be specified for the determination of the values of the model parameters (Table 1).

In this work, we have modeled relatively small tumors (5 mm diameter). Scaling up to larger tumors would require an increase in dose of at least an order of magnitude. Taking these considerations into account, at least five orders of magnitude increase in dose would be necessary to achieve the improvements in distribution shown in Fig. 4A. This dose would be orders of magnitude beyond what has been used in human clinical trials (1). Such a high dose would likely compromise the safety of an oncolytic HSV vector and would most certainly be impractical to obtain, given the relative difficulty of purifying HSV at high titers.

In conclusion, our results suggest that there are two efficient ways one can improve penetration of HSV virus in tumors. This can be achieved by either decreasing the affinity of binding to the cell surface through alterations of the viral envelope, or by increasing the diffusive transport of the virus through modifications of the interstitial space.

#### Translational Relevance

Oncolytic viruses offer a promising approach to the treatment of solid tumors. However, their effectiveness is often limited by insufficient distribution throughout the tumor. Here, we develop a mathematical model that provides insight into the causes of this inadequate distribution. We use parameters estimated from our own experiments and those of others to describe the processes of viral binding, interstitial transport, and degradation for herpes simplex virus (HSV). In strong agreement with our previous *in vivo* findings, the model predicts that infused HSV vectors will not spread significantly from the injection site. Importantly, we use this model to evaluate two methods for improving viral distribution and efficacy: (a) decreasing the affinity of HSV for its cell surface receptor and (b) modulating the extracellular matrix. We show that the combined effect of such changes would lead to a 3-fold or greater increase in the number of infected cells in the area surrounding the injection site.

### Supplementary Material

Refer to Web version on PubMed Central for supplementary material.

## Acknowledgments

We thank Drs. Gang Cheng, William Deen, Cornel Fraefel, Paola Grandi, Lance Munn, Xandra Breakefield, and Matthew Nugent for helpful discussions.

**Grant support:** National Cancer Institute (PO1CA80124 and RO1CA85140; R.K. Jain).

## References

1. Liu TC, Galanis E, Kirn D. Clinical trial results with oncolytic virotherapy: a century of promise, a decade of progress. *Nat Clin Pract Oncol* 2007;4:101–17. [PubMed: 17259931]
2. Jain RK. The next frontier of molecular medicine: delivery of therapeutics. *Nat Med* 1998;4:655–7. [PubMed: 9623964]
3. Sauthoff H, Hu J, Maca C, et al. Intratumoral spread of wild-type adenovirus is limited after local injection of human xenograft tumors: virus persists and spreads systemically at late time points. *Hum Gene Ther* 2003;14:425–33. [PubMed: 12691608]
4. van Etten B, ten Hagen TL, de Vries MR, Ambagtsheer G, Huet T, Eggermont AM. Prerequisites for effective adenovirus mediated gene therapy of colorectal liver metastases in the rat using an intracellular neutralizing antibody fragment to p21-Ras. *Br J Cancer* 2002;86:436–42. [PubMed: 11875712]
5. Yuan F, Leunig M, Huang SK, Berk DA, Papahadjopoulos D, Jain RK. Microvascular permeability and interstitial penetration of sterically stabilized (stealth) liposomes in a human tumor xenograft. *Cancer Res* 1994;54:3352–6. [PubMed: 8012948]
6. McKee TD, Grandi P, Mok W, et al. Degradation of fibrillar collagen in a human melanoma xenograft improves the efficacy of an oncolytic herpes simplex virus vector. *Cancer Res* 2006;66:2509–13. [PubMed: 16510565]
7. Netti PA, Berk DA, Swartz MA, Grodzinsky AJ, Jain RK. Role of extracellular matrix assembly in interstitial transport in solid tumors. *Cancer Res* 2000;60:2497–503. [PubMed: 10811131]
8. Tao Y, Guo Q. The competitive dynamics between tumor cells, a replication-competent virus and an immune response. *J Math Biol* 2005;51:37–74. [PubMed: 15772825]
9. Wein LM, Wu JT, Kirn DH. Validation and analysis of a mathematical model of a replication-competent oncolytic virus for cancer treatment: implications for virus design and delivery. *Cancer Res* 2003;63:1317–24. [PubMed: 12649193]
10. Wodarz D. Viruses as antitumor weapons: defining conditions for tumor remission. *Cancer Res* 2001;61:3501–7. [PubMed: 11309314]
11. Pluen A, Boucher Y, Ramanujan S, et al. Role of tumor-host interactions in interstitial diffusion of macromolecules: cranial vs. subcutaneous tumors. *Proc Natl Acad Sci U S A* 2001;98:4628–33. [PubMed: 11274375]
12. Shukla D, Spear PG. Herpesviruses and heparan sulfate: an intimate relationship in aid of viral entry. *J Clin Invest* 2001;108:503–10. [PubMed: 11518721]
13. Herold BC, Visalli RJ, Susmarski N, Brandt CR, Spear PG. Glycoprotein C-independent binding of herpes simplex virus to cells requires cell surface heparan sulphate and glycoprotein B. *J Gen Virol* 1994;75:1211–22. [PubMed: 8207388]
14. Shieh MT, WuDunn D, Montgomery RI, Esko JD, Spear PG. Cell surface receptors for herpes simplex virus are heparan sulfate proteoglycans. *J Cell Biol* 1992;116:1273–81. [PubMed: 1310996]
15. WuDunn D, Spear PG. Initial interaction of herpes simplex virus with cells is binding to heparan sulfate. *J Virol* 1989;63:52–8. [PubMed: 2535752]
16. Rux AH, Lou H, Lambris JD, Friedman HM, Eisenberg RJ, Cohen GH. Kinetic analysis of glycoprotein C of herpes simplex virus types 1 and 2 binding to heparin, heparan sulfate, and complement component C3b. *Virology* 2002;294:324–32. [PubMed: 12009874]
17. Williams RK, Straus SE. Specificity and affinity of binding of herpes simplex virus type 2 glycoprotein B to glycosaminoglycans. *J Virol* 1997;71:1375–80. [PubMed: 8995662]

18. Herold BC, WuDunn D, Soltys N, Spear PG. Glycoprotein C of herpes simplex virus type 1 plays a principal role in the adsorption of virus to cells and in infectivity. *J Virol* 1991;65:1090–8. [PubMed: 1847438]
19. Laquerre S, Argnani R, Anderson DB, Zucchini S, Manservigi R, Glorioso JC. Heparan sulfate proteoglycan binding by herpes simplex virus type 1 glycoproteins B and C, which differ in their contributions to virus attachment, penetration, and cell-to-cell spread. *J Virol* 1998;72:6119–30. [PubMed: 9621076]
20. Thurber GM, Witttrup KD. Quantitative spatiotemporal analysis of antibody fragment diffusion and endocytic consumption in tumor spheroids. *Cancer Res* 2008;68:3334–41. [PubMed: 18451160]
21. Nemunaitis J, Khuri F, Ganly I, et al. Phase II trial of intratumoral administration of ONYX-015, a replication-selective adenovirus, in patients with refractory head and neck cancer. *J Clin Oncol* 2001;19:289–98. [PubMed: 11208818]
22. Baxter LT, Jain RK. Transport of fluid and macromolecules in tumors. I. Role of interstitial pressure and convection. *Microvasc Res* 1989;37:77–104. [PubMed: 2646512]
23. Gerlowski LE, Jain RK. Microvascular permeability of normal and neoplastic tissues. *Microvasc Res* 1986;31:288–305. [PubMed: 2423854]
24. Mok W, Boucher Y, Jain RK. Matrix metalloproteinases-1 and -8 improve the distribution and efficacy of an oncolytic virus. *Cancer Res* 2007;67:10664–8. [PubMed: 18006807]
25. Chary SR, Jain RK. Direct measurement of interstitial convection and diffusion of albumin in normal and neoplastic tissues by fluorescence photobleaching. *Proc Natl Acad Sci U S A* 1989;86:5385–9. [PubMed: 2748592]
26. Phillips RJ, Deen WM, Brady JF. Hindered transport in fibrous membranes and gels. *AIChE J* 1989;35:1761–9.
27. Solomentsev YE, Anderson JL. Rotation of a sphere in Brinkman fluids. *Phys Fluids* 1996;8:1119–21.
28. Griffon-Etienne G, Boucher Y, Brekken C, Suit HD, Jain RK. Taxane-induced apoptosis decompresses blood vessels and lowers interstitial fluid pressure in solid tumors: clinical implications. *Cancer Res* 1999;59:3776–82. [PubMed: 10446995]
29. Ramanujan S, Pluen A, McKee TD, Brown EB, Boucher Y, Jain RK. Diffusion and convection in collagen gels: implications for transport in the tumor interstitium. *Biophys J* 2002;83:1650–60. [PubMed: 12202388]
30. Sodeik B, Ebersold MW, Helenius A. Microtubule-mediated transport of incoming herpes simplex virus 1 capsids to the nucleus. *J Cell Biol* 1997;136:1007–21. [PubMed: 9060466]
31. Day YS, Baird CL, Rich RL, Myszka DG. Direct comparison of binding equilibrium, thermodynamic, and rate constants determined by surface- and solution-based biophysical methods. *Protein Sci* 2002;11:1017–25. [PubMed: 11967359]
32. Deinum J, Gustavsson L, Gyzander E, Kullman-Magnusson M, Edstrom A, Karlsson R. A thermodynamic characterization of the binding of thrombin inhibitors to human thrombin, combining biosensor technology, stopped-flow spectrophotometry, and microcalorimetry. *Anal Biochem* 2002;300:152–62. [PubMed: 11779106]
33. Oddie GW, Gruen LC, Odgers GA, King LG, Kortt AA. Identification and minimization of nonideal binding effects in BIAcore analysis: ferritin/anti-ferritin Fab' interaction as a model system. *Anal Biochem* 1997;244:301–11. [PubMed: 9025947]
34. Roos H, Karlsson R, Nilshans H, Persson A. Thermodynamic analysis of protein interactions with biosensor technology. *J Mol Recognit* 1998;11:204–10. [PubMed: 10076841]
35. Krol A, Maresca J, Dewhirst MW, Yuan F. Available volume fraction of macromolecules in the extravascular space of a fibrosarcoma: implications for drug delivery. *Cancer Res* 1999;59:4136–41. [PubMed: 10463619]
36. Knipe, DM.; Howley, PM. *Fields Virology*. 5. Lippincott Williams and Wilkins; 2007.
37. Willis SH, Rux AH, Peng C, et al. Examination of the kinetics of herpes simplex virus glycoprotein D binding to the herpesvirus entry mediator, using surface plasmon resonance. *J Virol* 1998;72:5937–47. [PubMed: 9621056]
38. Brown E, McKee T, diTomaso E, et al. Dynamic imaging of collagen and its modulation in tumors *in vivo* using second-harmonic generation. *Nat Med* 2003;9:796–800. [PubMed: 12754503]

39. Bakay L. The extracellular space in brain tumours. I. Morphological considerations. *Brain* 1970;93:693–8. [PubMed: 4321422]
40. Gullino PM, Grantham FH, Smith SH. The interstitial water space of tumors. *Cancer Res* 1965;25:727–31. [PubMed: 14347560]
41. O'Connor SW, Bale WF. Accessibility of circulating immunoglobulin G to the extravascular compartment of solid rat tumors. *Cancer Res* 1984;44:3719–23. [PubMed: 6744289]
42. Cai WZ, Person S, Warner SC, Zhou JH, DeLuca NA. Linker-insertion nonsense and restriction-site deletion mutations of the gB glycoprotein gene of herpes simplex virus type 1. *J Virol* 1987;61:714–21. [PubMed: 3027398]
43. Post DE, Fulci G, Chiocca EA, Van Meir EG. Replicative oncolytic herpes simplex viruses in combination cancer therapies. *Curr Gene Ther* 2004;4:41–51. [PubMed: 15032613]
44. Jain RK. Delivery of molecular and cellular medicine to solid tumors. *Adv Drug Deliv Rev* 2001;46:149–68. [PubMed: 11259838]
45. Currier MA, Adams LC, Mahller YY, Cripe TP. Widespread intratumoral virus distribution with fractionated injection enables local control of large human rhabdomyosarcoma xenografts by oncolytic herpes simplex viruses. *Cancer Gene Ther* 2005;12:407–16. [PubMed: 15665822]
46. Bobo RH, Laske DW, Akbasak A, Morrison PF, Dedrick RL, Oldfield EH. Convection-enhanced delivery of macromolecules in the brain. *Proc Natl Acad Sci U S A* 1994;91:2076–80. [PubMed: 8134351]
47. Boucher Y, Brekken C, Netti PA, Baxter LT, Jain RK. Intratumoral infusion of fluid: estimation of hydraulic conductivity and implications for the delivery of therapeutic agents. *Br J Cancer* 1998;78:1442–8. [PubMed: 9836476]
48. Nagano S, Perentes JY, Jain RK, Boucher Y. Cancer cell death enhances the penetration and efficacy of oncolytic herpes simplex virus in tumors. *Cancer Res* 2008;68:3795–802. [PubMed: 18483263]
49. Dingwell KS, Brunetti CR, Hendricks RL, et al. Herpes simplex virus glycoproteins E and I facilitate cell-to-cell spread *in vivo* and across junctions of cultured cells. *J Virol* 1994;68:834–45. [PubMed: 8289387]
50. Wang Y, Hu JK, Krol A, Li YP, Li CY, Yuan F. Systemic dissemination of viral vectors during intratumoral injection. *Mol Cancer Ther* 2003;2:1233–42. [PubMed: 14617797]

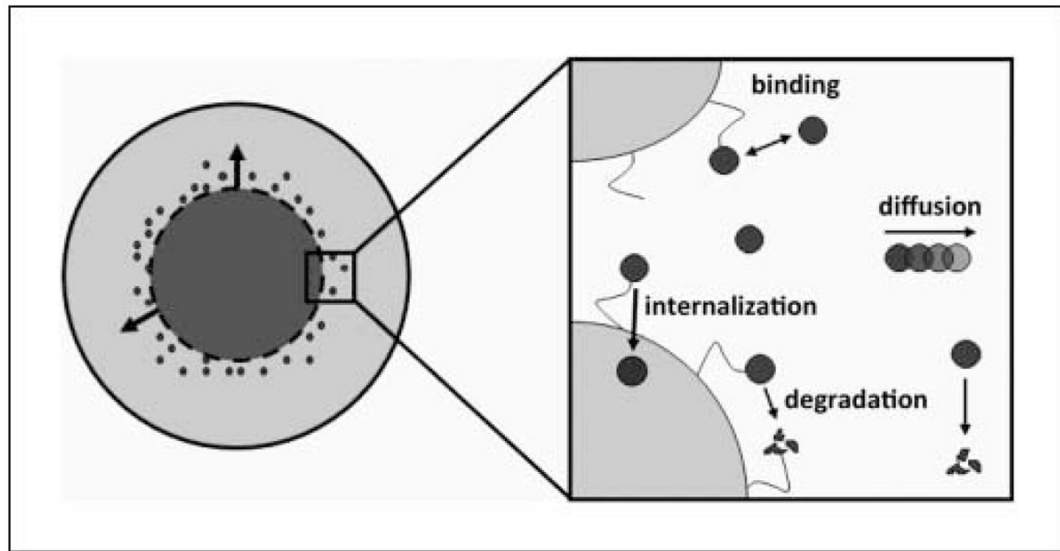


**Fig. 1.** Schematic diagram of model. The tumor is modeled as a sphere. Initially, virus is uniformly distributed in a spherical volume at the center of the tumor. Over time, virus spreads into the adjacent space. The four processes considered are as follows: (a) association and dissociation of virus and cell surface herapan sulfate; (b) degradation of free and bound virus; (c) diffusion of free virus; and (d) internalization of bound virus.

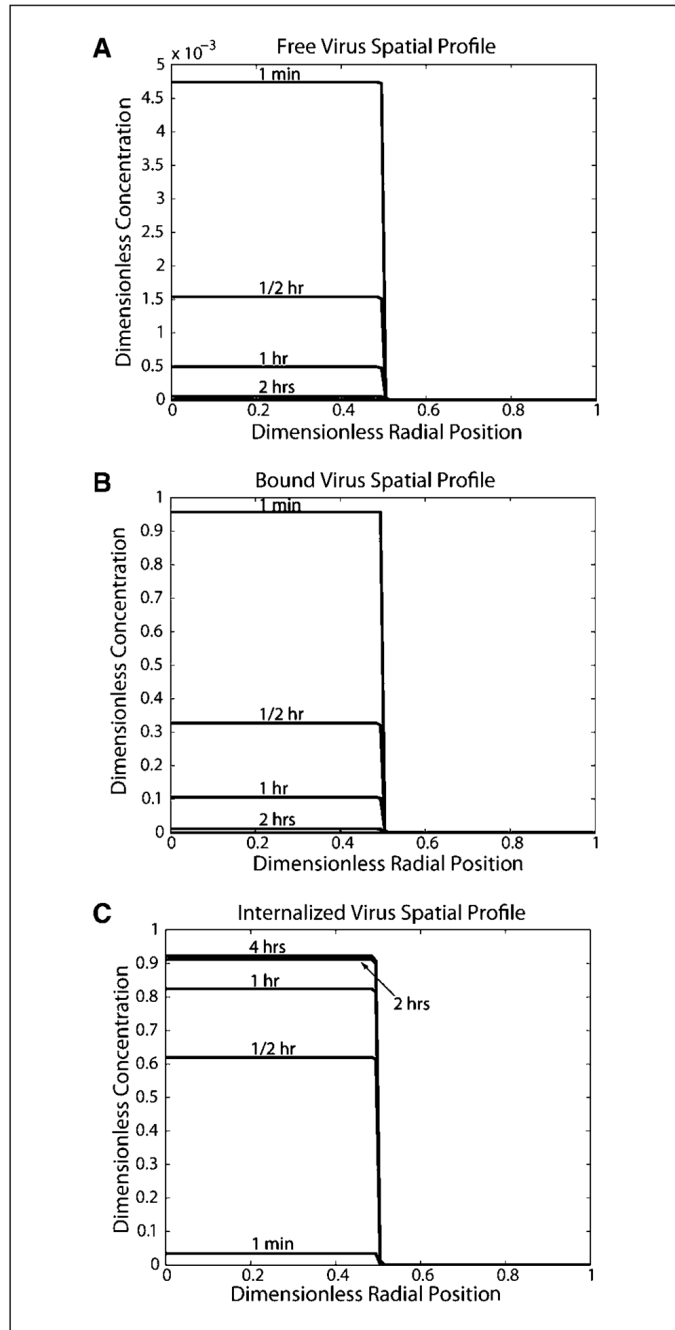


**Fig. 2.** Spatial profiles for free, bound, and internalized virus using baseline parameter values. Virus concentrations have been normalized to the initial free viral concentration in the injection site. The radial position has been normalized to the tumor radius (with 0 being the tumor center, 0.5 being the edge of the initial injection site, and 1.0 being the tumor edge). *A*, free virus spatial profile. *B*, bound virus spatial profile. *C*, internalized virus spatial profile.

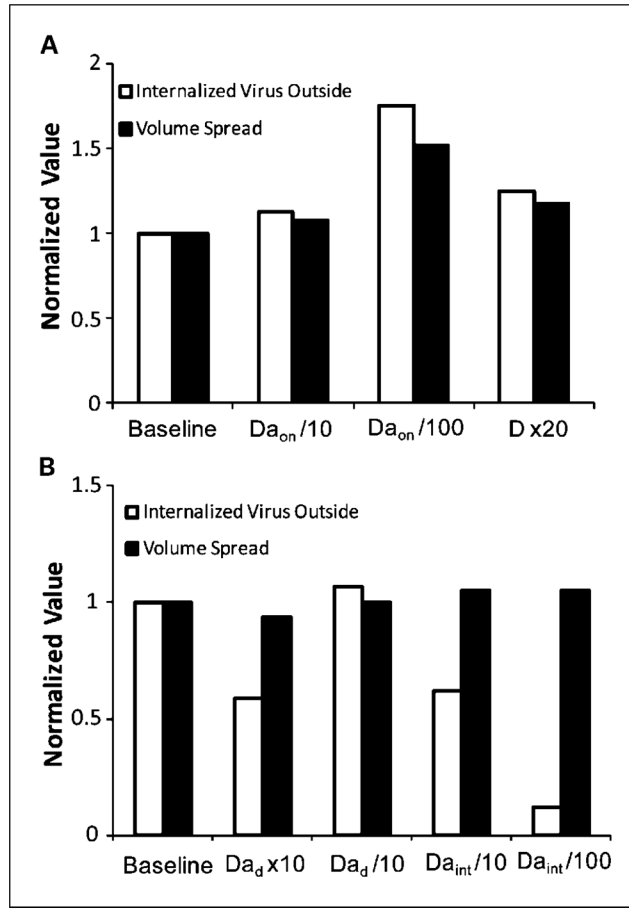


**Fig. 3.**

Effect of parameter modifications on internalized virus concentration and spread volume. The values for the total concentration of internalized virus outside the initial distribution volume and the spread volume are shown, normalized to the values in the baseline simulation. Concentrations are at 4 hours after the beginning of the simulation and spread volumes are maximum values. *A*, effect of changes in the binding kinetics and diffusion coefficient on virus distribution. A decrease in the binding affinity or an increase in the diffusion coefficient increases the spread volume significantly. *B*, effect of changes in the degradation and internalization rate constant on viral distribution. An increase in the degradation rate or decrease in the internalization rate result in a significant decrease in the amount of virus but has no effect on the spread volume.

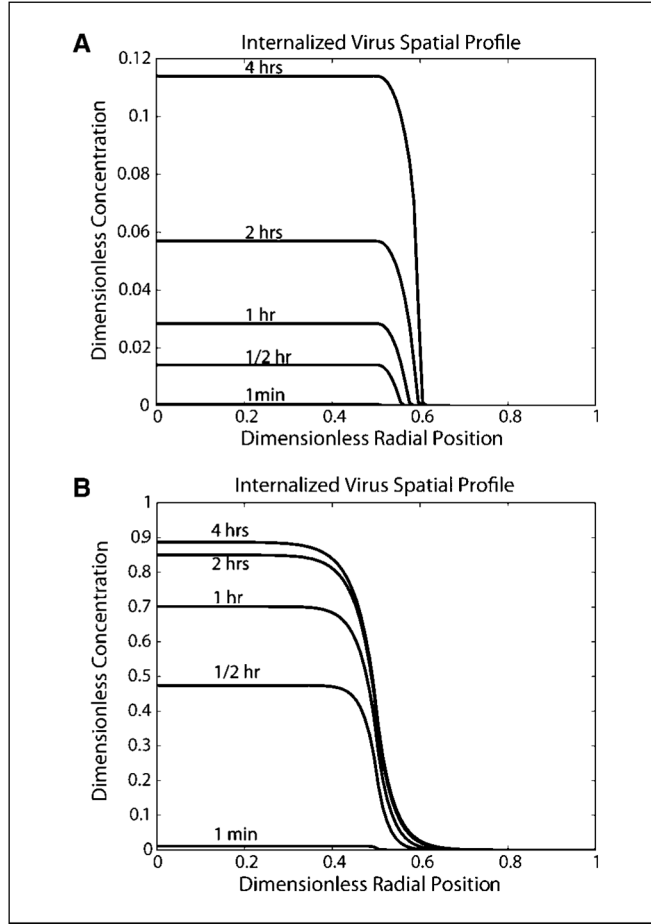


**Fig. 4.** Spatial profiles for internalized virus using adjusted parameter values. *A*, model simulation with the initial dose increased 1,000-fold, whereas all other parameters are kept at their baseline value. Virus behaves as a moving front of internalized virus into the adjacent space as receptors in the initial injection volume have been saturated. *B*, model simulation with the diffusion coefficient increased by a factor of 10, and  $Da_{on}$  decreased by a factor of 100, with all other parameters kept at their baseline value. Significant diffusion into the adjacent volume occurs.

**Table 1**

## Baseline model parameters

| Symbol    | Definition                                      | Value                             |
|-----------|---|-----------------------------------|
| $D$       | Diffusion coefficient                           | $5E-10 \text{ cm}^2\text{s}^{-1}$ |
| $k_{on}$  | Association rate constant                       | $5E3 \text{ M}^{-1}\text{s}^{-1}$ |
| $k_{off}$ | Dissociation rate constant                      | $8E-3 \text{ s}^{-1}$             |
| $k_d$     | Degradation rate constant                       | $4.8E-5 \text{ s}^{-1}$           |
| $k_{int}$ | Internalization rate constant                   | $5.78E-4 \text{ s}^{-1}$          |
| $C_0$     | Initial virus concentration in injection volume | $1.27E-9 \text{ M}$               |
| $R$       | Radius of tumor                                 | $5E-2 \text{ cm}$                 |
| $P$       | Radius of initial viral injection               | $2.5E-2 \text{ cm}$               |
| $\phi$    | Volume fraction of tumor accessible to virus    | 0.05                              |
| $C_{HS}$  | Heparan sulfate concentration                   | $1.74E-5 \text{ M}$               |
| $a$       | Heparan sulfate molecules per bound virus       | 1E3                               |

Table 2

## Sensitivity analysis

| Simulation                | Virus inside (# viral particles) | Virus outside (# viral particles) | Virus inside (normalized) | Virus outside (normalized) | Spread volume (normalized) |
|---------------------------|----------------------------------|-----------------------------------|---------------------------|----------------------------|----------------------------|
| Baseline                  | $4.61 \times 10^7$               | $1.43 \times 10^6$                | 1.00                      | 1.00                       | 1.00                       |
| $Da_{off}/10$             | $4.57 \times 10^7$               | $1.61 \times 10^6$                | 0.99                      | 1.13                       | 1.08                       |
| $Da_{off}/100$            | $4.32 \times 10^7$               | $2.51 \times 10^6$                | 0.94                      | 1.76                       | 1.52                       |
| $Da_d \times 10$          | $2.72 \times 10^7$               | $8.42 \times 10^5$                | 0.59                      | 0.59                       | 0.94                       |
| $Da_d \phi/10$            | $4.95 \times 10^7$               | $1.54 \times 10^6$                | 1.07                      | 1.07                       | 1.00                       |
| $Da_{inff}/10$            | $2.69 \times 10^7$               | $8.92 \times 10^5$                | 0.58                      | 0.62                       | 1.05                       |
| $Da_{inff}/100$           | $4.81 \times 10^6$               | $1.66 \times 10^5$                | 0.10                      | 0.12                       | 1.05                       |
| $D \times 20$             | $4.57 \times 10^7$               | $1.78 \times 10^6$                | 0.99                      | 1.25                       | 1.18                       |
| $\phi \times 3$           | $4.61 \times 10^7$               | $1.48 \times 10^6$                | 1.00                      | 1.03                       | 1.00                       |
| $\phi/3$                  | $4.61 \times 10^7$               | $1.42 \times 10^6$                | 1.00                      | 1.00                       | 0.94                       |
| $C_o \times 100$          | $3.61 \times 10^9$               | $4.62 \times 10^8$                | 78.3                      | 323.1                      | 1.18                       |
| $C_o \times 1,000$        | $1.42 \times 10^{10}$            | $6.34 \times 10^9$                | 308.0                     | 443.8                      | 1.6                        |
| $Dx10$ and $Da_{off}/10$  | $4.47 \times 10^7$               | $2.64 \times 10^6$                | 0.97                      | 1.85                       | 1.52                       |
| $Dx10$ and $Da_{off}/100$ | $3.97 \times 10^7$               | $6.08 \times 10^6$                | 0.86                      | 4.25                       | 3.57                       |

NOTE: Values for changes in  $Da_{off}$  are nearly equivalent to values for opposite and proportional changes in  $Da_{on}$ .